Functional characterization of a Na^+-dependent dicarboxylate transporter from *Vibrio cholerae*

Christopher Mulligan,[1] Gabriel A. Fitzgerald,[1] Da-Neng Wang,[2,3] and Joseph A. Mindell[1]

[1]Membrane Transport Biophysics Section, Porter Neuroscience Research Center, National Institute of Neurological Disorders and Stroke, National Institutes of Health, Bethesda, MD 20892
[2]The Helen L. and Martin Kimmel Center for Biology and Medicine, Skirball Institute of Biomolecular Medicine and [3]Department of Cell Biology, New York University School of Medicine, New York, NY 10016

The SLC13 transporter family, whose members play key physiological roles in the regulation of fatty acid synthesis, adiposity, insulin resistance, and other processes, catalyzes the transport of Krebs cycle intermediates and sulfate across the plasma membrane of mammalian cells. SLC13 transporters are part of the divalent anion:Na^+ symporter (DASS) family that includes several well-characterized bacterial members. Despite sharing significant sequence similarity, the functional characteristics of DASS family members differ with regard to their substrate and coupling ion dependence. The publication of a high resolution structure of dimer VcINDY, a bacterial DASS family member, provides crucial structural insight into this transporter family. However, marrying this structural insight to the current functional understanding of this family also demands a comprehensive analysis of the transporter's functional properties. To this end, we purified VcINDY, reconstituted it into liposomes, and determined its basic functional characteristics. Our data demonstrate that VcINDY is a high affinity, Na^+-dependent transporter with a preference for C_4- and C_5-dicarboxylates. Transport of the model substrate, succinate, is highly pH dependent, consistent with VcINDY strongly preferring the substrate's dianionic form. VcINDY transport is electrogenic with succinate coupled to the transport of three or more Na^+ ions. In contrast to succinate, citrate, bound in the VcINDY crystal structure (in an inward-facing conformation), seems to interact only weakly with the transporter in vitro. These transport properties together provide a functional framework for future experimental and computational examinations of the VcINDY transport mechanism.

The Journal of General Physiology

INTRODUCTION

In humans, members of the SLC13 transporter family catalyze the transport of dicarboxylic and tricarboxylic acids, as well as sulfate, across the plasma membrane, fulfilling several physiological and pathophysiological roles (Bergeron et al., 2013). Citrate plays a major role in determining the metabolic status of the cell by acting as a key precursor and allosteric regulator of fatty acid synthesis (Spencer and Lowenstein, 1962), and by down-regulating both fatty acid β-oxidation and glycolysis (Garland et al., 1963; Denton and Randle, 1966; Ruderman et al., 1999). NaDC1 (SLC13A2) is found on the apical membranes of renal proximal tubule and appears to be important for the regulation of urinary citrate and the prevention of kidney stones (Ho et al., 2007), whereas its high affinity homologue, NaDC3 (SLC13A3), has a wide tissue distribution (Pajor, 2014). NaCT (SLC13A5) is responsible, in part, for the uptake of citrate into the cytosol of liver cells (Inoue et al., 2002b,c). Remarkably, deletion of NaCT in mice leads to protection against adiposity and insulin resistance, highlighting the integral role of these transporters to normal metabolic function and hinting at therapeutic potential in combating metabolic disease, obesity, and diabetes (Birkenfeld et al., 2011). Members of the SLC13 family are ∼50% identical to each other and display distinct functional properties. NaCT is primarily a citrate transporter but can also transport C_4-dicarboxylates such as succinate, fumarate, and malate (Inoue et al., 2002b). NaDC1 and NaDC3 are C_4-dicarboxylate transporters with a low and high affinity, respectively, but also retain the ability to transport citrate (Pajor, 1995; Pajor and Sun, 1996, 2000; Kekuda et al., 1999; Oshiro and Pajor, 2005). Two other SLC13 members (NaS1 [SLC13A1] and NaS2 [SLC13A4]) transport, among other compounds, divalent anions sulfate and selenate (Busch et al., 1994; Markovich et al., 2005). Despite differences in substrate affinity and specificity, all five SLC13 members couple the electrogenic transport of their respective substrates to the transport of multiple Na^+ ions.

The SLC13 transporters belong to a larger group of related transporters called the divalent anion:Na^+ symporter (DASS) family (Transporter Classification Database no. 2.A.47) (Saier et al., 2006). Knockdown of a gene

Correspondence to Joseph A. Mindell: mindellj@ninds.nih.gov

Abbreviations used in this paper: DASS, divalent anion:Na^+ symporter; MM(PEG)12, methyl-PEG_{12}-maleimide.

The Rockefeller University Press $30.00
J. Gen. Physiol. Vol. 143 No. 6 745–759
www.jgp.org/cgi/doi/10.1085/jgp.201311141

encoding a DASS family member (I'm not dead yet [INDY]) in the fruit fly *Drosophila melanogaster* results in reduced fat storage and, interestingly, an extended lifespan phenotype, mimicking the effects of caloric restriction (Rogina et al., 2000). In contrast to its human counterparts, citrate and C_4-dicarboxylate transport by the fly homologue, DrINDY, is apparently electroneutral and cation independent (Knauf et al., 2002). Several bacterial DASS family members (~30% identical to human SLC13 family members) have also been studied, revealing functional characteristics sometimes similar but sometimes divergent compared with the human homologues. However, the similarities are sufficient to suggest a comparable architecture and shared basic mode of action (Hall and Pajor, 2007; Youn et al., 2008; Strickler et al., 2009; Pajor et al., 2013).

Recently, our understanding of the transport mechanism of this family took a significant step forward with the publication of a high resolution x-ray crystal structure of VcINDY, a SLC13 homologue from *Vibrio cholerae* (Mancusso et al., 2012) (Fig. 1, A and B). VcINDY is 26–33% identical to SLC13 family members in amino acid sequence and, like other DASS family members, couples a Na^+ gradient to the transport of succinate, a C_4-dicarboxylate, in cell-based assays (Mancusso et al., 2012). In these assays, transport of succinate is inhibited by the presence of other C_4-dicarboxylates, malate and fumarate, suggesting that they may also serve as substrates. On the other hand, citrate and glutamate only mildly inhibit succinate transport, whereas sulfate has no effect (Mancusso et al., 2012). Succinate, malate, and citrate also confer thermostability to the detergent-solubilized VcINDY protein (Mancusso et al., 2012), suggesting that all three compounds interact with the protein. The 3.2-Å resolution crystal structure of VcINDY reveals a homodimeric protein, with each protomer containing 11 transmembrane helices and 2 reentrant hairpin loops, HP_{IN} and HP_{OUT} (Fig. 1, A and B). In each protomer, conserved residues at the tips of HP_{IN} and HP_{OUT} coordinate the bound substrate, likely a single citrate molecule, and a single Na^+ ion. A second predicted Na^+-binding site lies at the tip of HP_{OUT}, but no Na^+ ion is detected at this location and the role of this putative binding site in Na^+ binding and transport has not been functionally verified (Mancusso et al., 2012). Topological studies of VcINDY homologues and the location of the substrates in the crystal structure suggest that this structure of VcINDY represents the inward-facing state of the protein (Mancusso et al., 2012) (Fig. 1 A). The bound citrate molecule has been proposed to be acting as a state-dependent inhibitor, trapping the protein in this inward-facing conformation, although there is little evidence to support this assertion. The structure and cell-based characterization of VcINDY clearly place it as a functional representative of the DASS family but leave key mechanistic questions unanswered, including those regarding its transport stoichiometry, the extent of its substrate selectivity, and its ion coupling.

Here, we address these functional questions for VcINDY by assaying the purified protein reconstituted into liposomes. Measuring transport activity using proteoliposomes has several advantages over using whole cells or membrane vesicles. In proteoliposomes, the protein of interest can be reconstituted in isolation, eliminating the possibility of artifacts caused by native transport activity in the bacterial cell or by interactions with endogenous bacterial proteins (Chen and Wilson, 1986; Quick et al., 2006; Hall and Pajor, 2007). In addition, unlike cells, the reconstituted system provides complete control of both external and internal solutions, and substrate catabolism is not a problem. Collectively, these features make the purified, reconstituted system an ideal setting for precise functional characterization of bacterial transporter proteins. Using this experimental approach, we demonstrate that VcINDY is a Na^+ gradient–dependent, electrogenic, pH gradient–independent C_4-dicarboxylate transporter with characteristics most similar to its mammalian homologue, NaDC3, the high affinity dicarboxylate transporter. These results are essential for further analysis of the transporter's mechanism and for initiating computational studies of VcINDY.

MATERIALS AND METHODS

Expression and purification

VcINDY was expressed and purified essentially as described previously (Mancusso et al., 2012). BL21-AI (Life Technologies) was transformed with pEThisINDY (a modified pET vector [Love et al., 2010] harboring the gene encoding VcINDY with an N-terminal deca-histidine tag) and grown in LB supplemented with 100 µg/ml kanamycin to A_{600} of 0.6, at which point expression was induced by the addition of 0.1 M IPTG and 6.6 mM (0.1% wt/vol) L-arabinose. Cultures were incubated overnight at 19°C and then harvested and lysed using a homogenizer (EmulsiFlex-C3; Avestin), and the membrane fraction was isolated by ultracentrifugation. This membrane fraction was resuspended in buffer containing 50 mM Tris HCl, pH 8, 100 mM NaCl, and 5% (vol/vol) glycerol. Protein was extracted from the membranes by the addition of *n*-dodecyl-β-D-maltoside (DDM; Anatrace) to a final concentration of 20 mM. Insoluble material was removed by ultracentrifugation, and the detergent-solubilized fraction was incubated with Talon metal affinity resin (Takara Bio Inc.) overnight at 4°C. The resin was washed, first with 20 column volumes (CV) of the above buffer supplemented with 2 mM DDM and 10 mM imidazole, and then with 20 CV of the same buffer supplemented with 2 mM DDM and 20 mM imidazole. Bound protein was eluted by the addition of buffer containing 300 mM imidazole. The histidine tag was removed by incubation with his-tagged TEV protease overnight at 4°C. The TEV protease and uncleaved protein were removed by reapplying the sample to Talon resin. The protein not sequestered by the resin was collected, concentrated, and exchanged into buffer containing 50 mM Tris/HEPES, pH 7.5, 150 mM NaCl, 5% glycerol, and 3 mM decyl-β-D-maltoside (DM; Anatrace). The protein was either used immediately or snap-frozen and stored at −80°C. Protein concentration was calculated using the absorbance at 280 nm and the theoretical extinction coefficient.

Protein reconstitution

Protein was functionally reconstituted into liposomes essentially as described previously for the aspartate transporter Glt_{Ph} (Ryan et al., 2009). Lipids, in a ratio of 3:1 *Escherichia coli* polar lipids to POPC (Avanti Polar Lipids, Inc.), were dried and resuspended to a concentration of 10 mg/ml in internal solution (the nature of the internal solution was dependent on the nature of the transport assay; typically, it was 20 mM Tris/HEPES, pH 7.5, 1 mM NaCl, and 199 mM KCl). After five freeze–thaw cycles, the lipids were extruded though a 400-nm filter and titrated with Triton X-100. The incorporation of Triton X-100 was monitored using the A_{540} reading, and additions were stopped after reaching the saturation point. Protein was added to the lipids in a ratio of 1.5 µg protein/mg lipid. The detergent was gradually removed, and proteoliposomes were formed by multiple additions of Biobeads SM (Bio-Rad Laboratories). The proteoliposomes were separated from the Biobeads, collected by centrifugation, resuspended to a final concentration of 10 mg/ml lipid with the appropriate lumenal solution, snap-frozen, and stored at −80°C. If the need arose to change the internal solution, the proteoliposomes were collected by centrifugation, diluted in the desired solution, freeze-thawed three times, and extruded.

Transport assays

Before performing the transport assays, the proteoliposomes were extruded through a 400-nm filter and concentrated to 100 mg/ml lipid by centrifugation. A typical transport assay was performed as follows. The transport reaction was started by 150-fold dilution of the proteoliposomes into appropriate reaction solution warmed to 30°C. The reaction solution varied depending on the experiment (see below for details), but for a typical transport assay, this solution consisted of 20 mM Tris/HEPES, pH 7.5, 100 mM KCl, 100 mM NaCl, 1 µM valinomycin, and 1 µM [^{3}H]succinate (American Radiolabeled Chemicals). For all transport assays performed, at each time point a 0.2-ml sample was taken and diluted 10-fold in ice-cold quench buffer consisting of 20 mM Tris/HEPES, pH 7.5, and 200 mM choline chloride (ChCl). The quenched reaction was then subjected to rapid filtration over a nitrocellulose membrane (0.22 µm; EMD Millipore), and the filters were washed with 3 ml of quench buffer. Each filter was dissolved in a liquid scintillation cocktail (FilterCount; PerkinElmer), and associated radioactivity was counted using a Trilux β counter (PerkinElmer). Initial transport rates were calculated using a linear fit to three points in the first minute of the transport reaction.

The composition of the solutions was changed depending on the requirements of the experiment. In the cation dependence experiment (Fig. 2), valinomycin was omitted and the Na^+ in the internal and external solutions was replaced with LiCl or KCl. ChCl was used to maintain the ionic and osmotic balance of the solutions. In the Na^+ dose–response experiment (Fig. 3), the internal solution contained 20 mM Tris/HEPES, pH 7.5, 1 mM NaCl, 200 mM KCl, and 99 mM ChCl. The external solution consisted of 20 mM Tris/HEPES, pH 7.5, 100 mM KCl, 2.5–300 mM NaCl, 1 µM valinomycin, and 1 µM [^{3}H]succinate. The kinetic parameters were derived by fitting the data with the Hill equation:

$$V = \frac{V_{max}[S]^b}{\left[K_{(0.05)}\right]^b + [S]^b},$$

where V is the initial rate, [S] is the substrate concentration (the concentration of the co-substrate is kept constant), and b is the Hill coefficient.

For the succinate dose–response curve (Fig. 6 A), the kinetic parameters were derived by fitting the data with the Hill equation and Michaelis–Menten equation:

$$V = \frac{V_{max}[S]}{K_m + [S]}.$$

For the pH dependence experiments (Fig. 7), transport assays were performed as detailed for the typical transport assay. The low pH values (pH 4–5) of the solutions were attained using a Tris/gluconate-buffering system, and the pH values of the rest were set with a Tris/MES-buffering system. For the electrogenicity experiment (Fig. 4 B), we set the different voltages across the membrane by varying the K^+ gradient across the membrane in the presence of valinomycin: −120 mV (100 mM_{IN}/1 mM_{OUT}), −50 mV (100 mM_{IN}/15 mM_{OUT}), 0 mV (100 mM_{IN}/100 mM_{OUT}), +50 mV (15 mM_{IN}/100 mM_{OUT}), and +120 mV (1 mM_{IN}/100 mM_{OUT}). For the counterflow assay (Fig. 5), the liposomes were loaded with 50 mM Tris/HEPES, pH 7.5, 100 mM NaCl, and 1 mM succinate. The external solution contained 50 mM Tris/HEPES, pH 7.5, 100 mM NaCl, 900 nM succinate, and 100 nM [^{3}H]succinate. This experiment was also performed in the absence of Na^+ ions, in which case the NaCl in the above solutions was replaced with ChCl. For the citrate dose–response experiment (Fig. 8 C), trisodium citrate was used to increase the concentration of citrate in the external solution. The Na^+ concentration and ionic balance were maintained by the addition of NaCl. The osmotic balance of the solutions was maintained using sucrose. The percentage of abundance of the various citrate and succinate protonation states was calculated using HySS2009 software (Alderighi et al., 1999).

Fluorescent labeling of single-cysteine mutants

To specifically label only internal cysteines (those facing the lumen of the liposome), proteoliposomes containing VcINDY mutants were first incubated with the membrane-impermeable cysteine-reactive reagent methyl-PEG_{12}-maleimide (MM(PEG)12; Thermo Fisher Scientific) for 20 min at room temperature to fully label external cysteine residues. The MM(PEG)12 reaction was quenched by the addition of 100 mM L-cysteine. Excess cysteine and MM(PEG)12 were removed by two washing steps in which the proteoliposomes were pelleted by centrifugation and resuspended in buffer devoid of the unwanted reagents. The proteoliposomes were solubilized in 2.6% (wt/vol) DM, and internal cysteine residues were fluorescently labeled by incubation with Alexa Fluor 488 C5 Maleimide (Life Technologies) for 2 h at room temperature in a solution comprised of 20 mM Tris/HEPES, pH 7.4, 199 mM KCl, and 1 mM NaCl. As a positive control and to obtain a "100% labeled" sample, the initial MMPEG12 protection step was excluded. Thus, after DM solubilization, all cysteines were available to fluorescently label. Proteoliposomes were run on SDS-PAGE gels, and fluorescently labeled protein was visualized by UV transillumination using Fluorchem E (Proteinsimple). Equal protein loading was assessed by subsequently staining the gels with Coomassie Brilliant Blue dye.

RESULTS

Functional reconstitution of VcINDY

To assess the transport characteristics of VcINDY, we purified the protein, reconstituted it into liposomes, and measured its transport characteristics. We purified detergent-solubilized VcINDY with a single immobilized metal affinity chromatography step using the N-terminal decahistidine tag (Fig. 1), subsequently removing the affinity tag and reconstituting the protein by adding it to Triton X-100–destabilized liposomes using the procedure

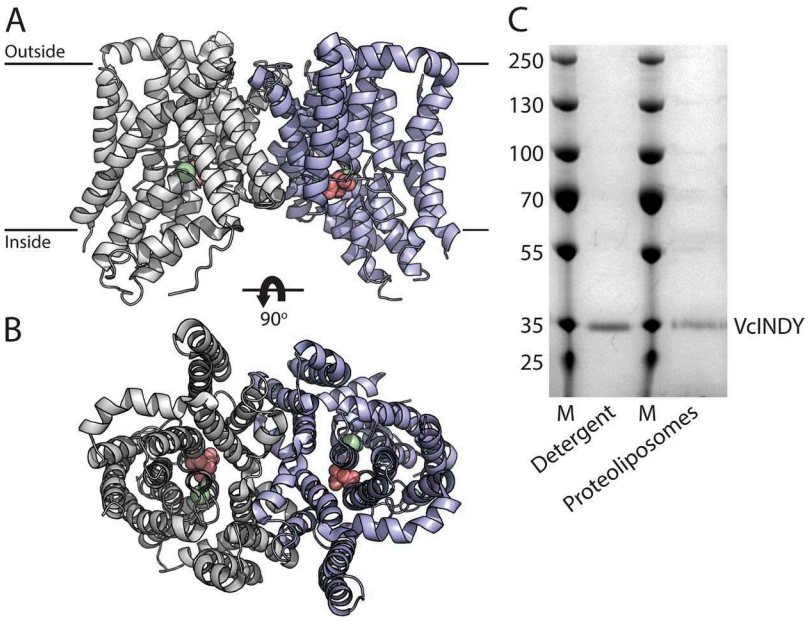

Figure 1. Purification and reconstitution of VcINDY. Crystal structure of VcINDY (Protein Data Bank accession no. 4F35) viewed from (A) within the plane of the membrane and (B) perpendicular to the membrane on the periplasmic side. One protomer is colored white, and the other is blue. The position of the bound citrate (pink spheres) and Na^+ ions (green spheres) is shown. (C) SDS-PAGE analysis of VcINDY after immobilized metal affinity chromatography purification (Detergent) and reconstitution into liposomes (Proteoliposomes). The band corresponding to VcINDY is labeled. Standard molecular weights (M) are indicated on the left of the gel.

established by Lévy et al. (1992). SDS-PAGE analysis of the resulting proteoliposomes revealed a single band at the same molecular weight as the protein purified in detergent solution (Fig. 1), confirming incorporation of the protein. Given the results of cell-based assays (Mancusso et al., 2012), we initially assessed function by measuring succinate uptake in our reconstituted system. Upon the application of an inwardly directed Na^+ gradient (100 mM outside, 1 mM inside), we observed rapid accumulation of the radiolabeled succinate into the lumen of the proteoliposomes (Fig. 2 A, closed circles). Under the same conditions, we found no accumulation of substrate for protein-free liposomes (not depicted), demonstrating that, as expected, VcINDY is responsible for catalyzing succinate transport. VcINDY-containing proteoliposomes did not accumulate substrate in the presence of equimolar concentrations of Na^+ on both sides of the membrane, revealing that a Na^+ gradient is required for succinate transport (Fig. 2, A and B, open triangles).

Cation specificity of succinate transport by VcINDY

All currently characterized members of the DASS family of transporters use an electrochemical Na^+ gradient to power transport of their respective substrates, with the exception of fly DrINDY and a vacuolar homologue from Arabidopsis (*At*tDT), both of which are cation independent (Inoue et al., 2002a; Knauf et al., 2002; Emmerlich et al., 2003). Li^+ has been shown to substitute for Na^+ in transport in some cases or to actually inhibit transport in others, with the best example of this being the rat and human orthologues of NaCT; the former is inhibited, whereas the latter is capable of Li^+-driven transport (Inoue et al., 2003). Previous whole cell transport assays suggest that VcINDY can efficiently couple transport of succinate to both Na^+ and Li^+ (at a concentration of 5 mM), but not K^+ (Mancusso et al., 2012). As noted, we observed rapid accumulation of succinate upon the application of an inwardly directed Na^+ (Fig. 2 A, closed circles). Replacing Na^+ with Li^+ results in measurable

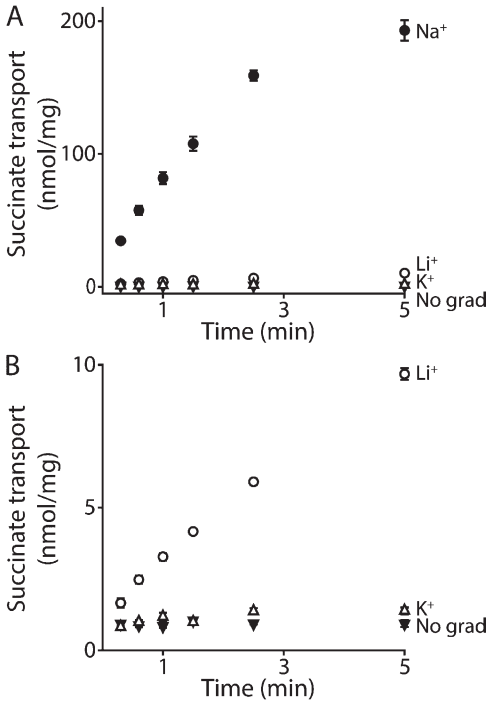

Figure 2. Cation specificity of VcINDY transport. (A) Transport of [^{3}H]succinate into VcINDY-containing liposomes in the presence of an inwardly directed Na^+ gradient (closed circles), Li^+ gradient (open circles), and K^+ gradient (closed triangles), or symmetrical [Na^+] (open triangles). (B) The same data as in A, but with the Na^+ gradient data removed to expand the scale and highlight Li^+-driven transport.

but vastly decreased transport that is only appreciable if plotted separately from the Na^+-dependent transport (Fig. 2 B, open circles). This result is surprising considering the above in vivo transport data that suggest almost equal efficacy of the two cations (Mancusso et al., 2012). Note though that those experiments were at much lower [Li^+] than ours, and that strong concentration dependence of transport to Li^+ has been observed previously for other SLC13 proteins (Pajor, 2006). A K^+ gradient is incapable of supporting transport via VcINDY (Fig. 2 B, closed triangles).

Na^+ dependence of succinate transport

The number of Na^+ ions coupled to transport varies among the members of the DASS family; most couple the transport of their respective substrate to three Na^+ ions (Busch et al., 1994; Kekuda et al., 1999; Wang et al., 2000; Dawson et al., 2005; Miyauchi et al., 2006), whereas some couple transport to two Na^+ ions (Markovich et al., 2005; Hall and Pajor, 2007; Pajor et al., 2013), and some to four (Inoue et al., 2002c). We investigated the number of Na^+ ions coupled to succinate transport by VcINDY by monitoring the transport rate of [^{3}H]succinate in the presence of varying external concentrations of Na^+. The succinate transport rate depends strongly on the external Na^+ concentration (Fig. 3). At 30°C, kinetic analysis revealed an apparent K_m for Na^+ of 41.7 ± 2.6 mM, a V_{max} of 53.5 ± 7.2 nmol/mg/min, and a Hill coefficient of 3.2 ± 0.3 (at 1 µM succinate), suggesting that three or more Na^+ ions are coupled to the transport of one succinate molecule. If indeed VcINDY couples the transport of one succinate to three (or more) Na^+ ions, we would expect net positive charge movement across the membrane during the transport cycle. The ensuing generation of an inside-positive membrane potential would inhibit further transport of [^{3}H]succinate. Under these circumstances, if a rate-limiting step in transport is voltage dependent, dissipation of this voltage using the K^+ ionophore valinomycin in the presence of K^+ should increase the initial succinate transport rate (given the lack of K^+ dependence of transport). Indeed, the addition of valinomycin resulted in a 2.5-fold increase in the initial rate of succinate transport, demonstrating that transport by VcINDY is electrogenic (Fig. 4 A). Furthermore, setting the membrane potential to values between −100 and +100 mV using K^+/valinomycin reveals variation in transport rates with the applied voltage (Fig. 4 B). We observed the highest transport rates at large negative membrane potentials, decreased rates at intermediate voltages, and the lowest rates at positive membrane potentials (Fig. 4 B). Collectively, these data demonstrate that transport of succinate is electrogenic and that at least one net positive charge is transferred into the liposome per transport cycle, suggesting that at least three Na^+ ions are coupled to the transport of one divalent succinate molecule per transport cycle.

The exchange reaction in a transporter monitors the binding of substrate and the outward facing to inward facing transition of the protein (Mulligan and Mindell, 2013). In theory, coupling between substrates (in a symporter like VcINDY) requires that only the empty or fully loaded transporter should be able to efficiently exchange between inward-facing and outward-facing states, otherwise coupling would be compromised (Stein, 1986). Thus,

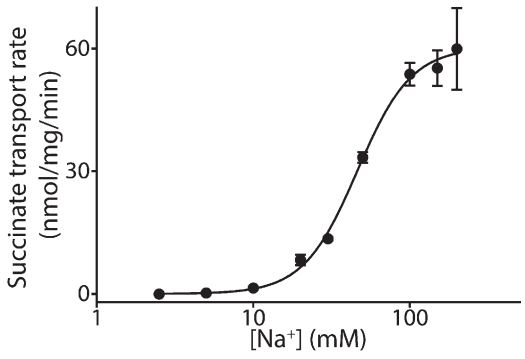

Figure 3. Na^+ dependence of [^{3}H]succinate transport activity. Initial rates of [^{3}H]succinate transport as a function of external Na^+ concentration. A triplicate dataset is averaged (error bars represent SEM) and fit to the Hill equation.

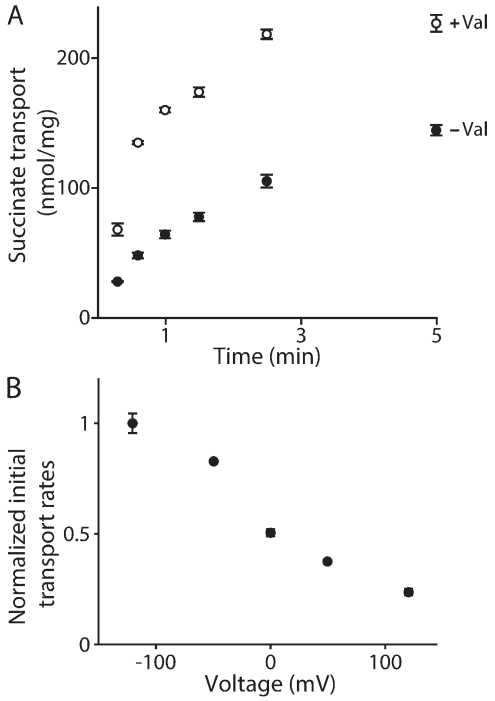

Figure 4. Electrical properties of VcINDY transport. (A) Transport of [^{3}H]succinate into VcINDY-containing liposomes in the presence of an inwardly directed Na^+ gradient in the presence (open circles, +Val) and absence (closed circles, −Val) of valinomycin. (B) Modulation of Na^+-dependent [^{3}H]succinate transport as a function of the voltage across the membrane set with K^+/valinomycin. Data are from triplicate datasets, and the error bars represent SEM.

the exchange reaction should require both coupled ions and substrate (the empty transporter, of course, will not mediate exchange of anything). We tested this prediction for VcINDY using a solute counterflow assay to monitor succinate exchange in the presence and absence of equimolar [Na^+] across the membrane (substituting with the nontransportable cation, choline). In this assay, the proteoliposomes are first loaded with a high concentration of unlabeled substrate and then diluted into an external solution containing a trace amount of [^{3}H]succinate. Stochastic, alternate sampling of the substrate-binding site to both sides of the membrane results in exchange of unlabeled substrate on the inside for radiolabeled substrate on the outside, resulting in uptake of the labeled substrate even without net change in its concentration (Kaczorowski and Kaback, 1979). In the presence of 100 mM Na^+ on both sides of the membrane, VcINDY catalyzes accumulation of [^{3}H]succinate (Fig. 5). However, we observe no exchange activity when Na^+ is replaced with choline. This result underscores the tight coupling of transport and supports a model where both Na^+ and succinate are simultaneously bound during substrate translocation, consistent with suggestions from the VcINDY crystal structure. Notably, a previously characterized bacterial orthologue of VcINDY, SdcS from *Staphylococcus aureus*, reportedly catalyzes Na^+-independent exchange of its substrate across the membrane, despite also being a Na^+ gradient–driven transporter (Hall and Pajor, 2007). If supported by further experiments, this finding may yield insight into the nature of the coupling mechanism.

Substrate specificity and kinetics of VcINDY

To explore the interaction between VcINDY and succinate, we monitored the succinate dose dependence of the initial transport rates in the presence of saturating (100 mM) concentrations of Na^+ (Fig. 6 A). This relation is well-fit by a hyperbolic curve, consistent with a single succinate-binding site per protomer. The parameters of the fit include apparent K_m of 1.0 ± 0.2 µM, V_{max} of 232.6 ± 17.2 nmol/mg/min, and a Hill coefficient of 0.88 ± 0.13 (30°C and a [Na^+] of 100 mM), and a turnover rate (K_{cat}) of 1.6 min^{-1}. This number represents a lower limit for the actual turnover rate but is accurate if all protein added to the reconstitution is active and is incorporated into liposomes and the vesicles are tight (Fig. 6 A). Collectively, these results are consistent with the presence of a noncooperative succinate-binding site and hint that the motions of the two protomers comprising the dimer are, to a first approximation, independent of one another.

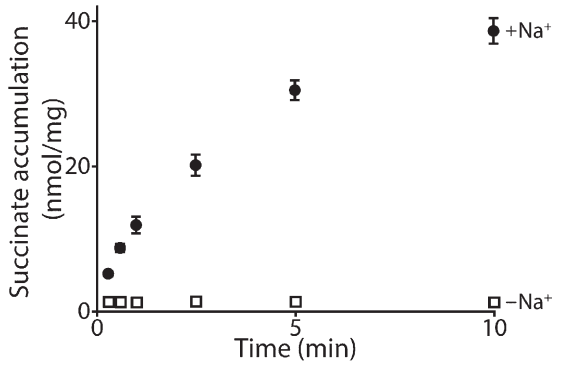

Figure 5. Solute counterflow activity of VcINDY. Solute counterflow activity of VcINDY-containing liposomes in the presence (closed circles, +Na^+) and absence (open squares, −Na^+) of Na^+. Data are from triplicate datasets, and the error bars represent SEM.

Previous characterization of a few candidate VcINDY substrates suggests that the transporter is capable of transporting succinate and at least interacting with malate and fumarate (Mancusso et al., 2012). Citrate confers enhanced thermostability (compared with the presence of no substrate) and is thought to be responsible for the electron density in the binding site of the crystal structure (Mancusso et al., 2012). We explored the substrate specificity of VcINDY using a competition assay in which we measured the transport of 1 µM [^{3}H]succinate in the presence of excess concentrations (1 mM) of 29 candidate substrates (Fig. 6 B). We observed strong inhibition of succinate transport in the presence of the C_4-darboxylates: succinate, malate, fumarate, and oxaloacetate (Fig. 6 C); succinate derivatives: 2,3-dimercaptosuccinate and mercaptosuccinate (but, interestingly, not 2,3-dimethylsuccinate); and the C_5-dicarboxylate: α-ketoglutarate. The binding site is clearly sensitive to the length of the carbon chain as neither shorter (oxalate (C_2) and malonate (C_3)) nor longer (glutarate (C_5), adipate (C_6), pimelate (C_7), and suberate (C_8)) dicarboxylates substantially inhibit succinate transport (Fig. 6 B). Maleate, the cis isomer of trans-butenedioic acid, has no inhibitory effects, unlike the trans isomer fumarate, showing that the transporter is isomer selective, a characteristic shared by other DASS members (Kekuda et al., 1999; Wang et al., 2000; Inoue et al., 2002a,c; Fei et al., 2003). We observe no inhibition by known substrates of NaS1 or NaS2 families: sulfate, selenate, thiosulfate, or dimercaptopropane-1-sulfonate (Busch et al., 1994; Markovich et al., 2005). Nor do we find effective inhibition of succinate transport by aspartate or glutamate, both of which interact with several DASS family members (Chen et al., 1998; Kekuda et al., 1999; Pajor and Sun, 2000; Wang et al., 2000; Strickler et al., 2009; Pajor et al., 2013). Inhibition of succinate transport implies an interaction between the transporter and the potential substrate. Although an alternative mechanism for inhibition, such as allosteric regulation, cannot be excluded based on this simple assay, the chemical similarity of the above candidates to succinate makes a competitive inhibition mechanism seem likely. Furthermore, this experiment does not allow us to discriminate between the inhibitors acting

by competitively binding to VcINDY versus being transported by the protein.

To establish which of these act as substrates and which merely inhibit the transport process, we evaluated several of these compounds for substrate activity by performing counterflow assays: loading vesicles with the candidate compound and diluting them into buffers containing small amounts of radiolabeled succinate. In these experiments, accumulation of radiolabeled succinate will only occur if VcINDY can transport the candidate compound. The results of this experiment are shown in Fig. 6 D. Clearly, VcINDY can transport fumarate, oxaloacetate, and malate, which, as shown above, are the most effective inhibitors of succinate transport. Gluconate, which did not inhibit succinate transport, is, as expected, not transported by VcINDY. In this experiment, fumarate showed the highest initial rate of uptake, followed by succinate/oxaloacetate then malate. Thus, VcINDY can catalyze the transport of several related dicarboxylate-containing compounds.

We also tested the inhibitory effect of several known DASS family inhibitors. Benzylpenicillin, which inhibits a NaDC3 homologue from winter flounder (Burckhardt et al., 2004), elicits no response when added to the transport reaction. Folate, although itself not a substrate of NaDC3, can modulate succinate-derived transport current (Burckhardt et al., 2005); in our hands, folate had a modest inhibitory effect on VcINDY transport. Flufenamic acid yields substantial inhibition of VcINDY transport (Fig. 6 B). This compound noncompetitively

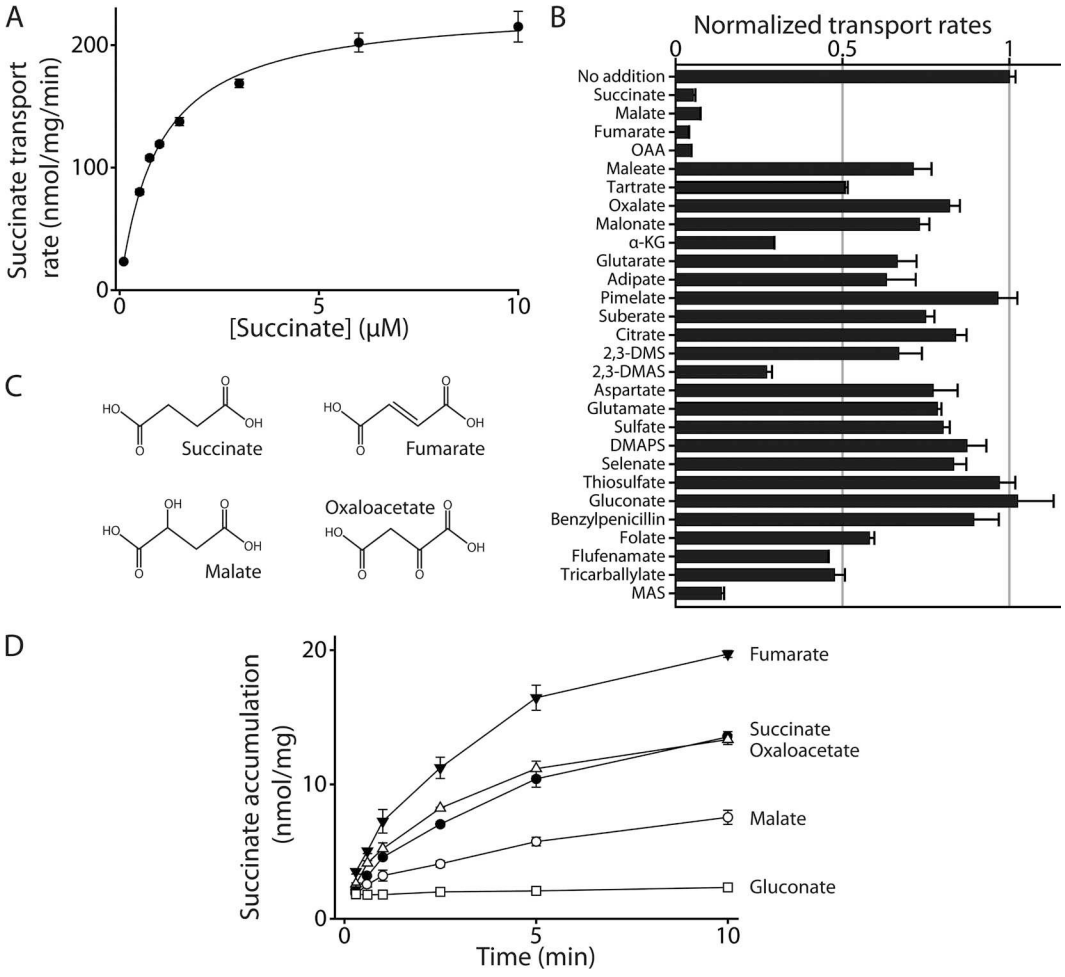

Figure 6. Substrate interactions with VcINDY. (A) Initial rates of [^{3}H]succinate transport as a function of external succinate concentration. The data are fit to the Michaelis–Menten equation. (B) Substrate specificity of VcINDY. Initial transport rate of [^{3}H]succinate into VcINDY-containing proteoliposomes in the presence of an inwardly directed Na^+ gradient at pH 7.5 and 29 potential substrates. Data for each competitor were normalized to the transport rate in the absence of competitor compound. OAA, oxaloacetate; α-KG, α-ketoglutarate; 2,3-DMS, 2,3-dimethylsuccinate; 2,3-DMAS, *Meso*-2,3-dimercaptosuccinate; DMAPS, dimercaptopropane-1-sulfonate; MAS, mercaptosuccinate. All data presented are the average from triplicate datasets, and the error bars represent SEM. (C) Chemical structures of the four most effective inhibitors: succinate, malate, fumarate, and oxaloacetate. (D) Solute counterflow activity of VcINDY-containing liposomes in the presence of 1-mM lumenal concentration of the most effective inhibitors identified in B: succinate (closed circles), malate (open circles), fumarate (closed triangles), and oxaloacetate (open triangles). Gluconate (open squares) is included as a negative control. All data presented are the average from triplicate datasets, and the error bars represent SEM.

inhibits both eukaryotic and bacterial DASS members (Burckhardt et al., 2004; Pajor and Sun, 2013), suggesting that the binding site for this particular inhibitor is preserved, despite the evolutionary distance between these transporters. Tricarballylate, a tricarboxylate similar in structure to citrate, inhibits transport. Citrate itself, however, does not inhibit transport at 1 mM under these conditions (Fig. 6 B, although see below for further assessment of high citrate concentrations).

pH dependence of succinate transport

Determining the charged state of the transported substrate is a key step in understanding the mechanism of VcINDY. Whether the substrate is neutral, singly, or doubly charged (or more than one of these) will affect the ability of the succinate to coordinate cotransported cations, influence the pH dependence of the transporter, and influence the coupling of transport to the membrane potential (via the net charge movement per transport cycle). Because succinate is a dicarboxylic acid with pKas within the range of pHs tested (4.21 and 5.64), the relative abundance of each protonation state of succinate varies with pH (Fig. 7, A–D, solid lines). By examining transport rates at varying external pHs, we can thereby control, to some extent, the relative fractions of the three charged forms of the substrate. While maintaining a pH_{INT} of 7.5, we observe that decreasing the pH_{EXT} from 7.5 to 5.5 decreases the transport rate, which (in this range) matches exactly the decrease in the relative abundance of fully deprotonated succinate (Fig. 7 A, $Succ^{2-}$, gray line), suggesting that $Succ^{2-}$ is the actual substrate of VcINDY. At lower pHs (4–5), the correlation between succinate accumulation rates and relative abundance of fully deprotonated succinate diverges with more substrate accumulating in the liposomes than predicted by the titration curve (Fig. 7 A). What is the cause of this divergence? One possibility is that there is proton-driven transport that is only observable at low pHs, which is unlikely given the lack of gradient dependence at higher pH. Alternatively, there could be a relative increase in the abundance of the monoprotonated and fully protonated states of succinate ($SuccH^{1-}$ and $SuccH_2$, respectively); at low pH, both of these, particularly the neutral form, are known to traverse the lipid bilayer itself (Kaim and Dimroth, 1998, 1999; Janausch et al., 2001). Upon internalization, the higher internal pH in the liposomes (7.5) would fully deprotonate $SuccH^{1-}$ and $SuccH_2$, trapping them and resulting in their accumulation. We tested this hypothesis by monitoring accumulation of [^{3}H]succinate into protein-free liposomes with an internal pH of 7.5 and varying the external pH between 4 and 7.5 (Fig. 7 D). At low external pH values, we observed substantial accumulation of succinate, accumulation that increased as the external pH decreased. This result validates the second hypothesis that the deviation from predicted transport

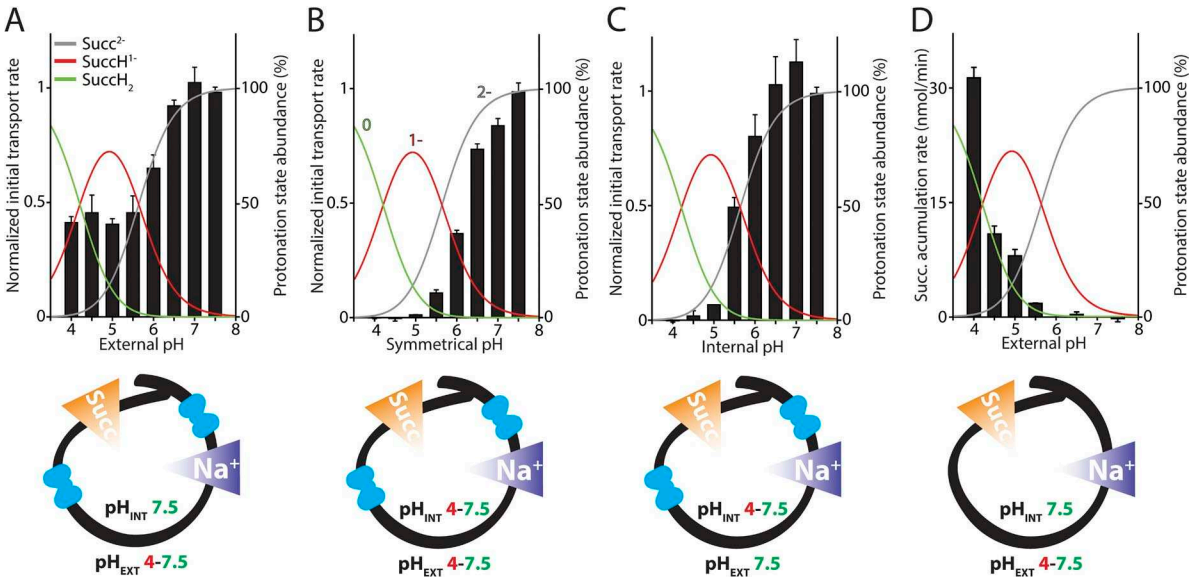

Figure 7. pH dependence of [^{3}H]succinate transport by VcINDY. The black bars represent the initial accumulation rates of [^{3}H]succinate into VcINDY-containing liposomes (A–C) and protein-free liposomes (D) under the following conditions: (A and D) fixed internal pH 7.5 and variable external pH, (B) symmetrical variation of pH, and (C) variable internal pH and fixed external pH 7.5. The line graphs represent the theoretical percentage of abundance of each protonation state of succinate (gray, deprotonated; red, monoprotonated; green, fully protonated) across the pH range used (percentage of abundance was calculated using HySS software; Alderighi et al., 1999). Below each panel is a schematic representation of the experimental conditions used; the thick black line represents the bilayer, the blue shapes represent VcINDY, and the internal and external pHs are noted. The orange and purple arrows indicate the presence of inwardly directed succinate and Na^+ gradients, respectively. All data presented are the average from triplicate datasets, and the error bars represent SEM.

rates is caused by direct membrane permeability of at least the neutral form of succinate and possibly its singly charged form as well. Indeed, the effects of the permeable succinate protonation states are also seen with fixed external pH 7.5 and varying internal pH. Although we observed robust transport at the higher internal pH, lowering the internal pH favored the membrane-permeant species and they diffused out of the liposomes, manifesting as an apparent lack of transport (Fig. 7 C). These results clearly demonstrate that only the doubly charged protonation state of succinate is transported by VcINDY. Our pH dependence experiments also reveal that VcINDY transport of succinate is not coupled to a proton gradient because the pH dependence of transport is essentially identical in the absence (Fig. 7 B) or presence of an inwardly directed (Fig. 7 A) or outwardly directed (Fig. 7 C) pH gradient (when we neglect the effects of direct succinate bilayer permeability).

Investigating the interactions between VcINDY and citrate

In our substrate competition assay, we observed no inhibition of succinate transport in the presence of 1 mM citrate (Fig. 6 B), a surprising result given the presumed citrate density in the crystal structure and the stabilizing effect of the ion on the folded protein (Mancusso et al., 2012). Comparing our transport conditions to those of crystallization, we found that the VcINDY was crystallized (in 100 mM citrate) at pH 6.5, whereas our competition assay was performed at pH 7.5. At pH 7.5, citrate is predominantly in its deprotonated state, citrate^{3-}, whereas at pH 6.5, half the citrate is citrate^{3-}, whereas the other half is citrateH^{2-} (Fig. 8 A, green and yellow block colors, respectively). Perhaps VcINDY only binds doubly charged anions, as we demonstrated is the case with succinate, which would explain why we observed no inhibition by citrate at pH 7.5 where the citrateH^{2-} protonation state is scarce. To test this, we monitored the transport of succinate in the presence of excess (1 mM) citrate at pH 7.5, 6.5, and 5.5. At pH 7.5, both succinate and citrate were almost fully deprotonated (Fig. 8 A, block colors, citrate; line data, succinate). At pH 6.5, however, a large population of citrate was dianionic and the majority of succinate was still deprotonated. At pH 5.5, ~80% of the citrate will be dianionic, whereas 50% of the deprotonated succinate will remain. If citrateH^{2-} binds and inhibits succinate transport by VcINDY, then lowering the pH should lead to observable inhibition. At the three different pH values, we observed no inhibitory effects of citrate on succinate transport, indicating that at this citrate concentration (1 mM), neither citrate^{3-} nor citrateH^{2-} interacts with VcINDY (Fig. 8 B). We investigated whether citrate simply binds at much lower affinity, by measuring succinate transport in the presence of increasing external concentrations of citrate. At pH 7.5, we observed 25% inhibition of transport activity at 75 mM citrate, the highest concentration we tested (Fig. 8 C, closed circles). At pH 5.5, where the dianionic form of citrate is most abundant, we observed no inhibitory effects of citrate at 10 mM; however, increasing the citrate concentration to 25 mM resulted in ~60% inhibition of succinate transport (Fig. 8 C, open

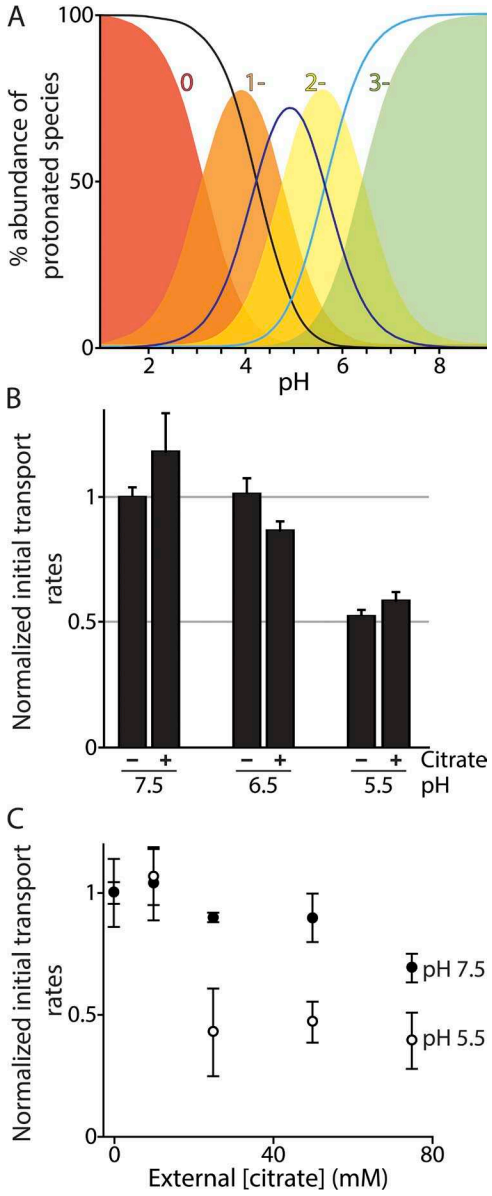

Figure 8. Citrate specificity of VcINDY. (A) Theoretical percentage of abundance of the protonation states of citrate (block colors: green, deprotonated; yellow, monoprotonated; orange, diprotonated; red, fully protonated) and succinate (lines: blue, deprotonated; purple, monoprotonated; black, fully protonated) as a function of pH (percentage of abundance was calculated using HySS software; Alderighi et al., 1999). (B) Normalized initial rate of succinate (final concentration of 1 µM with a radiolabeled to unlabeled ratio of 1:9) transport at pH 7.5, 6.5, and 5.5 in the presence (+) and absence (−) of 1,000-fold excess (1 mM) of citrate. (C) Initial rates of [^{3}H]succinate transport at pH 7.5 (closed circles) and 5.5 (open circles) as a function of citrate concentration. Data are from triplicate datasets, and the error bars represent SEM.

circles). Further increases in citrate concentration did not result in further inhibition (Fig. 8 C). Increased inhibition by citrate at the lower pH suggests that citrateH^{2-} does indeed interact with VcINDY, albeit with low affinity. Why do we see ~40% residual transport activity? If citrate is a competitive inhibitor that binds to VcINDY at the same site as succinate, one would expect complete inhibition of VcINDY transport activity upon adding sufficient excess of the ion. The fact that we do not see complete inhibition has a potentially simple explanation; if, as has been suggested (Mancusso et al., 2012), citrate is an inward-facing state-specific inhibitor of VcINDY, then its inhibitory efficacy would be dependent on the orientation of VcINDY in the membrane. If the orientation of VcINDY in the liposomes is mixed, i.e., VcINDY is present in the membrane in two populations, outside out (as it is oriented in vivo) and inside out, then citrate would only affect the population of VcINDY with its inner façade facing outward.

We addressed this issue by determining the orientation of VcINDY in the liposome membrane. We introduced single-cysteine residues into a cysteine-less version of VcINDY (cysless, each native cysteine was mutated to serine) at positions on either the cytoplasmic (A171C) or extracellular (V343C) faces of the protein (Fig. 9 A). Cysless VcINDY and the two single-cysteine mutants displayed measurable transport activity upon reconstitution into liposomes (Fig. 9 B). Because our fluorescent probe is somewhat membrane permeant (not depicted), we designed a multistep protocol to establish protein orientation. We treated all three mutants with the membrane-impermeable thiol-reactive reagent MM(PEG)12, solubilized the membrane, and labeled the remaining cysteines with the thiol-reactive fluorophore Alexa Fluor 488–maleimide. We analyzed the extent of labeling by separating the proteins using PAGE and imaging the gels while exciting the fluorophore with UV transillumination. Thus, only cysteine residues facing the lumen of the proteoliposomes, protected from MM(PEG)12 labeling, should be fluorescently labeled. The reactivity pattern of the two single-cysteine mutants suggests that VcINDY adopts a mixed orientation in the membrane (Fig. 9 C). First, both the internal site (V171C) and the external site (A343C) exhibited fluorescent labeling (Fig. 9 C, lane 1 for each mutant), indicating that both cysteines, despite being on opposite faces of the protein, were at least partially protected from MM(PEG)12 modification before membrane solubilization. Solubilizing the membrane before MM(PEG)12 labeling resulted in no fluorescent labeling (Fig. 9 C, lane 2); therefore, we are indeed fluorescently labeling the internally located cysteines. Second, excluding the MM(PEG)12 labeling step, solubilizing the membrane, and fluorescently labeling all available cysteines resulted in substantially greater fluorescent labeling (Fig. 9 C, lane 3), demonstrating that each cysteine, regardless of its position on the protein, can be exposed to either side of the membrane. These data reveal that the VcINDY protein incorporates in the liposome membrane in both possible orientations. Although our data are not quantitative enough to accurately determine the relative proportions of these orientations, they are consistent with a roughly equal distribution of both. In this context, our results on citrate inhibition are at least consistent with a sided mechanism of inhibition.

Does VcINDY have an uncoupled chloride conductance?

The VcINDY protomer is composed of two distinct domains: the scaffold domain, which forms all of the contacts at the dimer interface, and the transport domain, which houses all of the substrate-binding residues (Mancusso et al., 2012). This architecture is reminiscent of the EAAT homologue, Glt_{Ph}, whose structure and mechanism have been well studied (Yernool et al., 2004; Reyes et al., 2009; Hänelt et al., 2013; Jensen et al., 2013). During its transport cycle, Glt_{Ph} undergoes an elevator-type movement of the transport domain relative to the immobile scaffold domain (known as the trimerization domain in Glt_{Ph}), exposing the binding site from one side of the membrane to the other. Because of the architectural similarity between VcINDY and Glt_{Ph}, there is a possibility

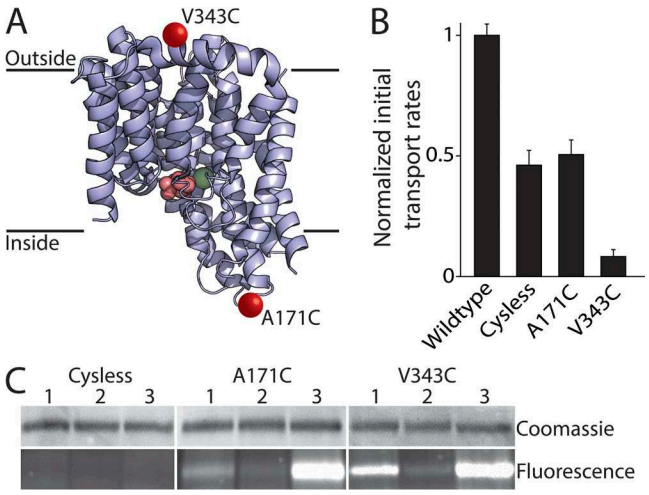

Figure 9. Determining the orientation of reconstituted VcINDY. (A) Structure of a single VcINDY protomer and its predicted positioning relative to the membrane. The positions of the external cysteine (V343C) and the internal cysteine (A171C, red spheres) are shown, as well as the bound citrate (pink spheres) and Na^+ ion (green sphere). (B) Initial transport rates of [^{3}H]succinate in the presence of an inwardly directed Na^+ gradient and liposomes containing wild-type VcINDY, cysteine-free VcINDY (cysless), VcINDYA171C, and VcINDYV343C. (C) Coomassie staining (top) and Alexa Fluor 448 labeling (bottom) of proteoliposomes containing the VcINDY mutants cysless, VcINDYA171C, and VcINDYV343C, treated as follows: (1) MM(PEG)12 treatment followed by solubilization and Alexa Fluor 448–maleimide treatment; (2) solubilization, MM(PEG)12 treatment, and Alexa Fluor 448–maleimide treatment; or (3) solubilization followed by Alexa Fluor 448-maleimide treatment.

that they share a similar mode of action, namely, an elevator-type mechanism. A characteristic of the EAATs and Glt_{Ph} is the presence of an uncoupled anion conductance, the pathway of which has been proposed to be located at the interface between the transport domain and the scaffold (Ryan and Mindell, 2007; Verdon and Boudker, 2012). If an uncoupled Cl^- conductance is a consequence of an elevator-like mechanism, this uncoupled anion conductance may also be shared. Several other DASS family members have been shown to exhibit interesting traits in the presence of anions, although not necessarily suggestive of an uncoupled chloride conductance (Inoue et al., 2002a; Oshiro and Pajor, 2005).

As we described previously, VcINDY-mediated transport of succinate is electrogenic: transport is enhanced by dissipating the membrane potential, as by valinomycin in Fig. 4. If VcINDY also carries an uncoupled Cl^- conductance, then Cl^- ion would also aid in dissipating the membrane potential, serving a role similar to that of valinomycin and thereby facilitating transport. In this case, replacing Cl^- with an impermeant anion should reduce transport rates, but only in the absence of valinomycin (Fig. 4), as was the case for Glt_{Ph} (Ryan and Mindell, 2007). We initially replaced chloride with gluconate and found, unexpectedly, that 100 mM gluconate is an excellent inhibitor of VcINDY (not depicted), despite exhibiting no inhibitory properties at lower concentrations (Fig. 6 B). We therefore substituted gluconate with another commonly used impermeable anion, methanesulfonate. Unfortunately, even methanesulfonate mildly inhibits VcINDY succinate transport. However, sufficient activity remains to evaluate the possibility of a Cl^- conductance. We see similar fractional inhibition when Cl^- is replaced by methanesulfonate in the presence or absence of valinomycin (Fig. 10), indicating that dissipating the membrane potential with the ionophore does not compensate for the absence of Cl^-. This, in turn, suggests that Cl^- is not itself dissipating the potential; it is not free to move across the membrane. This contrasts strongly with the observations reported for Glt_{Ph}, where the addition of valinomycin fully compensates for the inhibition caused by Cl^- replacement (Ryan and Mindell, 2007). Although the picture is somewhat clouded by the mild inhibition caused by methanesulfonate, these data suggest that the inhibition observed in the absence of valinomycin is caused by the presence of methanesulfonate rather than by the absence of chloride. This result therefore indicates that VcINDY does not have an uncoupled chloride conductance. However, it does further demonstrate that VcINDY is capable of interacting with several structurally unrelated anions.

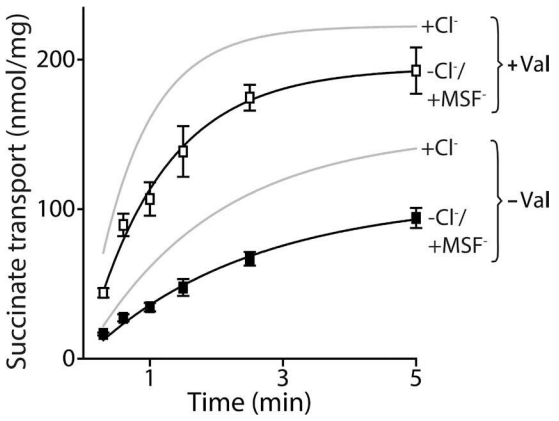

Figure 10. Chloride conductance of VcINDY. Transport of [^{3}H]succinate in the presence of chloride (+Cl^-, gray lines; data from Fig. 2 is redrawn) or methanesulfonate-containing buffers ($-Cl^{-/+}MSF^-$) in the presence (open symbols) and absence (closed symbols) of valinomycin. Data are fit to a single-exponential rise to max. Data are from triplicate datasets, and the error bars represent SEM.

DISCUSSION

The crystal structure of VcINDY represents the only high resolution structural information available for the DASS family of transporters. This study reports on the functional reconstitution and characterization of VcINDY to establish which transport features it shares with other DASS family members, including the physiologically important SLC13 family from humans. A detailed understanding of the transport mechanism of VcINDY will allow us to begin to understand the functional characteristics of other DASS family members from a structural viewpoint.

In accordance with the majority of functionally characterized DASS family members, VcINDY uses an electrochemical Na^+ gradient to power transport of the model substrate, succinate. A Li^+ gradient can substitute for the Na^+ gradient at 100 mM, but with a much lower relative efficacy compared with what was seen in cell-based assays at 5 mM Li^+ (Mancusso et al., 2012). This observed disparity between cell-based and liposome-based assays is likely caused by complications that arise from measuring transport in whole cells where the internal solution composition is hard to control and there are unknown contributions from endogenous transporters, as opposed to a purified and reconstituted system where a single protein is present and altering and maintaining the reaction solutions is trivial. The structure of VcINDY suggests a single substrate-binding site per protomer (Mancusso et al., 2012). This assertion is corroborated by kinetic analysis of succinate transport that revealed a hyperbolic dose–response curve and a Hill coefficient of 0.88, consistent with a single, noncooperative binding site for succinate. Under similar experimental conditions, although performed in whole cell assays or in membrane vesicles, two related bacterial transporters, SdcF and SdcS (30 and 32% identical to VcINDY, respectively), have sigmoidal dose–response curves, indicative of cooperative transport activity (Pajor

and Sun, 2013; Pajor et al., 2013). This finding suggests that either two substrate molecules bind to the same protomer, a notion inconsistent with our current structural understanding of this transporter family, or that the two protomers in a VcINDY dimer act cooperatively. Again, this observed sigmoidal activity may be a consequence of using whole cells and membrane vesicles in transport assays, as opposed to the purified and reconstituted system. Adding weight to this argument is the observation that purified and reconstituted SdcS has a Hill coefficient of 0.83, which is more in keeping with the apparently noncooperative transport we observe for VcINDY (Hall and Pajor, 2007). Although subunits in different DASS proteins may interact differently, our work points to each VcINDY protomer working independently.

The transport data presented here are inconsistent with a H^+ gradient contributing to transport; however, we found transport of succinate to be highly pH dependent. This mirrors the observations of pH-dependent transport for NaDC1 in whole cells (Wright et al., 1982). The decrease in succinate transport as pH dropped corresponds almost perfectly with the decrease in the theoretical abundance of $succinate^{2-}$ at higher pH, strongly suggesting that $succinate^{2-}$ is the actual substrate of VcINDY. In contrast, succinate transport by NaDC1 was completely insensitive to the solution pH, suggesting that the monoprotonated and deprotonated forms of succinate may both be transported (Pajor, 1995). NaDC3, however, is highly pH dependent, showing clearly that $succinate^{2-}$ is the only succinate protonation state transported (Kekuda et al., 1999). Of the other bacterial DASS members where the pH dependence of succinate transport has been studied, SdcL from *Bacillus licheniformis* was insensitive to pH (although the pH range tested was limited) (Strickler et al., 2009), and SdcS was sensitive, demonstrating that $succinate^{2-}$ is the preferred substrate here as well (Hall and Pajor, 2005). The protonation state of the substrate has profound effects on the transport mechanism, as it is fundamentally linked to the number of coupling ions transported and the electrogenicity of the transporter. The observation that $succinate^{2-}$ is the preferred protonation state, coupled with the fact that transport by VcINDY was electrogenic, demonstrates that at least three Na^+ ions are coupled to the transport of one $succinate^{2-}$. This stoichiometry is corroborated by kinetic analyses of both succinate and Na^+ dose–response curves that revealed Hill coefficients of 0.88 and 3.2, respectively. Although strictly these results establish three as the lower limit of the number of Na^+ ions, we suggest that the coupling stoichiometry is indeed three, consistent with the Hill coefficient and by analogy to other coupled transporters. Almost all of the DASS family members have a substrate/coupling ion stoichiometry of 1:3 (Busch et al., 1994; Chen et al., 1998; Kekuda et al., 1999; Miyauchi et al., 2006). The two exceptions are NaCT, which couples the transport of both $citrate^{3-}$ and $succinate^{2-}$ to four Na^+ ions (Inoue et al., 2002c), and all currently characterized bacterial homologues. Aside from VcINDY, all other bacterial homologues cotransport two Na^+ ions with succinate in an electroneutral process (Hall and Pajor, 2005, 2007; Strickler et al., 2009; Pajor et al., 2013). Of all the bacterial transporters characterized to date, VcINDY is the most similar to the mammalian homologues in both sequence and function and is therefore an excellent choice for a bacterial model of this family.

Aside from its apparent inability to transport citrate, the mechanism (electrogenicity, coupling ion stoichiometry) and substrate specificity of VcINDY most resemble the eukaryotic DASS members NaDC1 and NaDC3. The primary functional distinction between NaDC1 and NaDC3 is their K_m values; the former is considered low affinity, with a K_m range of 300–750 µM, and the latter is considered high affinity, with a K_m range of 2–20 µM. With a K_m value of 1 µM (the lowest K_m value reported for this family), VcINDY is most functionally similar to NaDC3 in this regard.

Our data suggests that citrate is capable of binding VcINDY, but only in its dianionic form and possibly only to one side of the protein. The first part of this conclusion is based on the observation that succinate transport is mainly affected by the presence of citrate at pH 5.5, where the majority of the citrate is dianionic, as opposed to pH 7.5, where the $citrate^{3-}$ is the predominant protonation state. In keeping with this, the crystal structure of VcINDY was captured at pH 6.5, where a large proportion of the 50 mM citrate present would be dianionic and therefore available to bind (Mancusso et al., 2012). However, inconsistent with this proposition is the observation that citrate confers considerable thermostability to VcINDY in pH 8.0 conditions, where only a small proportion of the citrate would be dianionic (Mancusso et al., 2012). This stabilizing effect may be explained by an allosteric interaction with citrate, but further work will be required to resolve this issue. Based on the crystal structure alone, citrate was proposed to be an inward-facing state inhibitor of VcINDY (Mancusso et al., 2012). Our results are consistent with this claim: we observed maximal inhibition of 50% regardless of how high we increased the citrate concentration, and we also demonstrate that the orientation of VcINDY in the liposomes is mixed. Further work is required to fully elaborate on the interaction between VcINDY and citrate. To date, VcINDY is the only bacterial DASS member to demonstrably interact with citrate (Hall and Pajor, 2005, 2007; Youn et al., 2008; Strickler et al., 2009; Pajor et al., 2013). The observed interaction with $citrate^{2-}$, although not actual transport, further strengthens the functional similarity between VcINDY and NaDC1 and NaDC3, both of which transport citrate and prefer the doubly charged form (Kekuda et al., 1999; Wang et al., 2000). NaCT, on the other hand,

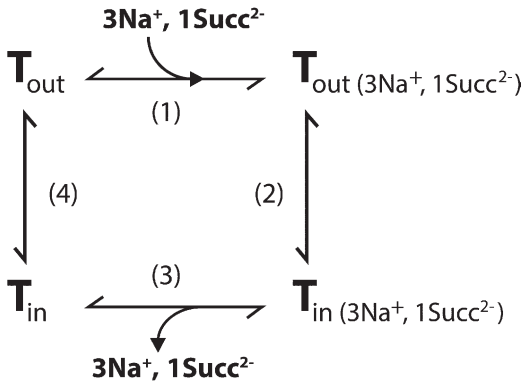

Figure 11. Simple transport scheme for VcINDY. In the outward-facing state, VcINDY binds three Na^+ ions and a single succinate molecule in an unknown order (1). The substrate-bound protein transitions from the outward- to the inward-facing state, presumably via an occluded state (2). Substrate is released in an unknown order into the cytoplasm, culminating in an empty, inward-facing state of the protein (3). The empty protein reverts to the starting position by transitioning from the inward-facing state to the outward-facing state (4).

transports the trianionic form of citrate (Inoue et al., 2002b,c, 2004).

Although our functional assays lack the resolution to dissect the order of substrate binding, we can suggest the following simple transport scheme based on extrapolation from other Na^+-dependent transporters (Fig. 11): (a) VcINDY, in the outward-facing state, binds one to three Na^+ ions, which induces formation of a favorable binding site for succinate^{2-}, which binds, followed by any remaining Na^+ ions; (b) VcINDY reorients from the outward-facing state to the inward-facing state (a conformation that resembles the current crystal structure), presumably via an occluded state; (c) Na^+ ion and succinate are released in an unknown order; and (d) empty transporter reorients back to the outward-facing state to begin the cycle anew. Specific predictions of such an ordered mechanism can be tested experimentally in the future.

The coupling of succinate transport to three Na^+ ions is advantageous to both *V. cholerae*, which uses succinate as a nutrient, and in the other physiological settings in which DASS family members are found. As succinate is transported in its divalent form, cotransport of three (or more) Na^+ ions makes the process electrogenic, allowing the negative membrane potential to help drive transport in addition to the Na^+ gradient. When the transport process reaches equilibrium, the final succinate concentration in the cell will be proportional to the cube of the Na^+ gradient, namely, $([Na^+]_{out}/Na^+]_{in})^3$ (Stein, 1986), which is much higher than that of a cotransporter with a Na^+ substrate ratio of 1 or 2 can possibly achieve.

The functional characterization of VcINDY presented here lays the groundwork to bridge the gap between the structural insight gained from this bacterial transporter and the function of its eukaryotic counterparts. Our results are also essential prerequisites for any computational examinations of binding or transport in VcINDY. This work demonstrates that many of the functional properties of mammalian DASS family members are retained in VcINDY, making it an excellent model for future structural and mechanistic studies on this family of transporters.

We thank Dr. Romina Mancusso for helpful discussions, Jinmei Song and Bining Lu for preliminary experiments in whole cells, and Lucy Forrest and Kenton Swartz for critical readings of the manuscript.

This work was supported by the Intramural Research Program of the National Institutes of Health (NIH), National Institute of Neurological Disorders and Stroke, and NIH grants (R01-DK099023, R01-DK073973, R01-GM093825, R01-DA019676, and U54-GM095315).

The authors declare no competing financial interests.

Merritt C. Maduke served as editor.

Submitted: 3 December 2013
Accepted: 21 April 2014

REFERENCES

Alderighi, L., P. Gans, A. Ienco, D. Peters, A. Sabatini, and A. Vacca. 1999. Hyperquad simulation and speciation (HySS): a utility program for the investigation of equilibria involving soluble and partially soluble species. *Coord. Chem. Rev.* 184:311–318. http://dx.doi.org/10.1016/S0010-8545(98)00260-4

Bergeron, M.J., B. Clémençon, M.A. Hediger, and D. Markovich. 2013. SLC13 family of Na^+-coupled di- and tri-carboxylate/sulfate transporters. *Mol. Aspects Med.* 34:299–312. http://dx.doi.org/10.1016/j.mam.2012.12.001

Birkenfeld, A.L., H.Y. Lee, F. Guebre-Egziabher, T.C. Alves, M.J. Jurczak, F.R. Jornayvaz, D. Zhang, J.J. Hsiao, A. Martin-Montalvo, A. Fischer-Rosinsky, et al. 2011. Deletion of the mammalian INDY homolog mimics aspects of dietary restriction and protects against adiposity and insulin resistance in mice. *Cell Metab.* 14:184–195. http://dx.doi.org/10.1016/j.cmet.2011.06.009

Burckhardt, B.C., J. Lorenz, G. Burckhardt, and J. Steffgen. 2004. Interactions of benzylpenicillin and non-steroidal anti-inflammatory drugs with the sodium-dependent dicarboxylate transporter NaDC-3. *Cell. Physiol. Biochem.* 14:415–424. http://dx.doi.org/10.1159/000080357

Burckhardt, B.C., J. Lorenz, C. Kobbe, and G. Burckhardt. 2005. Substrate specificity of the human renal sodium dicarboxylate cotransporter, hNaDC-3, under voltage-clamp conditions. *Am. J. Physiol. Renal Physiol.* 288:F792–F799. http://dx.doi.org/10.1152/ajprenal.00360.2004

Busch, A.E., S. Waldegger, T. Herzer, J. Biber, D. Markovich, H. Murer, and F. Lang. 1994. Electrogenic cotransport of Na^+ and sulfate in *Xenopus* oocytes expressing the cloned $Na^+SO4(2-)$ transport protein NaSi-1. *J. Biol. Chem.* 269:12407–12409.

Chen, C.C., and T.H. Wilson. 1986. Solubilization and functional reconstitution of the proline transport system of *Escherichia coli*. *J. Biol. Chem.* 261:2599–2604.

Chen, X.Z., C. Shayakul, U.V. Berger, W. Tian, and M.A. Hediger. 1998. Characterization of a rat Na^+-dicarboxylate cotransporter. *J. Biol. Chem.* 273:20972–20981. http://dx.doi.org/10.1074/jbc.273.33.20972

Dawson, P.A., K.J. Pirlo, S.E. Steane, K.A. Nguyen, K. Kunzelmann, Y.J. Chien, and D. Markovich. 2005. The rat Na^+-sulfate cotransporter

rNaS2: functional characterization, tissue distribution, and gene (*slc13a4*) structure. *Pflugers Arch.* 450:262–268. http://dx.doi.org/10.1007/s00424-005-1414-6

Denton, R.M., and P.J. Randle. 1966. Citrate and the regulation of adipose-tissue phosphofructokinase. *Biochem. J.* 100:420–423.

Emmerlich, V., N. Linka, T. Reinhold, M.A. Hurth, M. Traub, E. Martinoia, and H.E. Neuhaus. 2003. The plant homolog to the human sodium/dicarboxylic cotransporter is the vacuolar malate carrier. *Proc. Natl. Acad. Sci. USA.* 100:11122–11126. http://dx.doi.org/10.1073/pnas.1832002100

Fei, Y.J., K. Inoue, and V. Ganapathy. 2003. Structural and functional characteristics of two sodium-coupled dicarboxylate transporters (ceNaDC1 and ceNaDC2) from *Caenorhabditis elegans* and their relevance to life span. *J. Biol. Chem.* 278:6136–6144. http://dx.doi.org/10.1074/jbc.M208763200

Garland, P.B., P.J. Randle, and E.A. Newsholme. 1963. Citrate as an intermediary in the inhibition of phosphofructokinase in rat heart muscle by fatty acids, ketone bodies, pyruvate, diabetes, and starvation. *Nature.* 200:169–170. http://dx.doi.org/10.1038/200169a0

Hall, J.A., and A.M. Pajor. 2005. Functional characterization of a Na^+-coupled dicarboxylate carrier protein from *Staphylococcus aureus*. *J. Bacteriol.* 187:5189–5194. http://dx.doi.org/10.1128/JB.187.15.5189-5194.2005

Hall, J.A., and A.M. Pajor. 2007. Functional reconstitution of SdcS, a Na^+-coupled dicarboxylate carrier protein from *Staphylococcus aureus*. *J. Bacteriol.* 189:880–885. http://dx.doi.org/10.1128/JB.01452-06

Hänelt, I., D. Wunnicke, E. Bordignon, H.J. Steinhoff, and D.J. Slotboom. 2013. Conformational heterogeneity of the aspartate transporter Glt(Ph). *Nat. Struct. Mol. Biol.* 20:210–214. http://dx.doi.org/10.1038/nsmb.2471

Ho, H.T., B.C. Ko, A.K. Cheung, A.K. Lam, S. Tam, S.K. Chung, and S.S. Chung. 2007. Generation and characterization of sodium-dicarboxylate cotransporter-deficient mice. *Kidney Int.* 72:63–71. http://dx.doi.org/10.1038/sj.ki.5002258

Inoue, K., Y.J. Fei, W. Huang, L. Zhuang, Z. Chen, and V. Ganapathy. 2002a. Functional identity of *Drosophila melanogaster* Indy as a cation-independent, electroneutral transporter for tricarboxylic acid-cycle intermediates. *Biochem. J.* 367:313–319. http://dx.doi.org/10.1042/BJ20021132

Inoue, K., L. Zhuang, and V. Ganapathy. 2002b. Human Na^+-coupled citrate transporter: primary structure, genomic organization, and transport function. *Biochem. Biophys. Res. Commun.* 299:465–471. http://dx.doi.org/10.1016/S0006-291X(02)02669-4

Inoue, K., L. Zhuang, D.M. Maddox, S.B. Smith, and V. Ganapathy. 2002c. Structure, function, and expression pattern of a novel sodium-coupled citrate transporter (NaCT) cloned from mammalian brain. *J. Biol. Chem.* 277:39469–39476. http://dx.doi.org/10.1074/jbc.M207072200

Inoue, K., L. Zhuang, D.M. Maddox, S.B. Smith, and V. Ganapathy. 2003. Human sodium-coupled citrate transporter, the orthologue of *Drosophila* Indy, as a novel target for lithium action. *Biochem. J.* 374:21–26. http://dx.doi.org/10.1042/BJ20030827

Inoue, K., Y.J. Fei, L. Zhuang, E. Gopal, S. Miyauchi, and V. Ganapathy. 2004. Functional features and genomic organization of mouse NaCT, a sodium-coupled transporter for tricarboxylic acid cycle intermediates. *Biochem. J.* 378:949–957. http://dx.doi.org/10.1042/BJ20031261

Janausch, I.G., O.B. Kim, and G. Unden. 2001. DctA- and Dcu-independent transport of succinate in *Escherichia coli*: contribution of diffusion and of alternative carriers. *Arch. Microbiol.* 176:224–230. http://dx.doi.org/10.1007/s002030100317

Jensen, S., A. Guskov, S. Rempel, I. Hänelt, and D.J. Slotboom. 2013. Crystal structure of a substrate-free aspartate transporter. *Nat. Struct. Mol. Biol.* 20:1224–1226. http://dx.doi.org/10.1038/nsmb.2663

Kaczorowski, G.J., and H.R. Kaback. 1979. Mechanism of lactose translocation in membrane vesicles from *Escherichia coli*. 1. Effect of pH on efflux, exchange, and counterflow. *Biochemistry.* 18:3691–3697. http://dx.doi.org/10.1021/bi00584a009

Kaim, G., and P. Dimroth. 1998. Voltage-generated torque drives the motor of the ATP synthase. *EMBO J.* 17:5887–5895. http://dx.doi.org/10.1093/emboj/17.20.5887

Kaim, G., and P. Dimroth. 1999. ATP synthesis by F-type ATP synthase is obligatorily dependent on the transmembrane voltage. *EMBO J.* 18:4118–4127. http://dx.doi.org/10.1093/emboj/18.15.4118

Kekuda, R., H. Wang, W. Huang, A.M. Pajor, F.H. Leibach, L.D. Devoe, P.D. Prasad, and V. Ganapathy. 1999. Primary structure and functional characteristics of a mammalian sodium-coupled high affinity dicarboxylate transporter. *J. Biol. Chem.* 274:3422–3429. http://dx.doi.org/10.1074/jbc.274.6.3422

Knauf, F., B. Rogina, Z. Jiang, P.S. Aronson, and S.L. Helfand. 2002. Functional characterization and immunolocalization of the transporter encoded by the life-extending gene Indy. *Proc. Natl. Acad. Sci. USA.* 99:14315–14319. http://dx.doi.org/10.1073/pnas.222531899

Lévy, D., A. Gulik, A. Bluzat, and J.L. Rigaud. 1992. Reconstitution of the sarcoplasmic reticulum Ca^{2+}-ATPase: mechanisms of membrane protein insertion into liposomes during reconstitution procedures involving the use of detergents. *Biochim. Biophys. Acta.* 1107:283–298. http://dx.doi.org/10.1016/0005-2736(92)90415-I

Love, J., F. Mancia, L. Shapiro, M. Punta, B. Rost, M. Girvin, D.N. Wang, M. Zhou, J.F. Hunt, T. Szyperski, et al. 2010. The New York Consortium on Membrane Protein Structure (NYCOMPS): a high-throughput platform for structural genomics of integral membrane proteins. *J. Struct. Funct. Genomics.* 11:191–199. http://dx.doi.org/10.1007/s10969-010-9094-7

Mancusso, R., G.G. Gregorio, Q. Liu, and D.N. Wang. 2012. Structure and mechanism of a bacterial sodium-dependent dicarboxylate transporter. *Nature.* 491:622–626. http://dx.doi.org/10.1038/nature11542

Markovich, D., R.R. Regeer, K. Kunzelmann, and P.A. Dawson. 2005. Functional characterization and genomic organization of the human Na^+-sulfate cotransporter hNaS2 gene (SLC13A4). *Biochem. Biophys. Res. Commun.* 326:729–734. http://dx.doi.org/10.1016/j.bbrc.2004.11.102

Miyauchi, S., S.R. Srinivas, Y.J. Fei, E. Gopal, N.S. Umapathy, H. Wang, S.J. Conway, V. Ganapathy, and P.D. Prasad. 2006. Functional characteristics of NaS2, a placenta-specific Na^+-coupled transporter for sulfate and oxyanions of the micronutrients selenium and chromium. *Placenta.* 27:550–559. http://dx.doi.org/10.1016/j.placenta.2005.05.004

Mulligan, C., and J.A. Mindell. 2013. Mechanism of transport modulation by an extracellular loop in an archaeal excitatory amino acid transporter (EAAT) homolog. *J. Biol. Chem.* 288:35266–35276. http://dx.doi.org/10.1074/jbc.M113.508408

Oshiro, N., and A.M. Pajor. 2005. Functional characterization of high-affinity Na^+/dicarboxylate cotransporter found in *Xenopus laevis* kidney and heart. *Am. J. Physiol. Cell Physiol.* 289:C1159–C1168. http://dx.doi.org/10.1152/ajpcell.00295.2004

Pajor, A.M. 1995. Sequence and functional characterization of a renal sodium/dicarboxylate cotransporter. *J. Biol. Chem.* 270:5779–5785.

Pajor, A.M. 2006. Molecular properties of the SLC13 family of dicarboxylate and sulfate transporters. *Pflugers Arch.* 451:597–605. http://dx.doi.org/10.1007/s00424-005-1487-2

Pajor, A.M. 2014. Sodium-coupled dicarboxylate and citrate transporters from the SLC13 family. *Pflugers Arch.* 466:119–130. http://dx.doi.org/10.1007/s00424-013-1369-y

Pajor, A.M., and N. Sun. 1996. Functional differences between rabbit and human Na^+-dicarboxylate cotransporters, NaDC-1 and hNaDC-1. *Am. J. Physiol.* 271:F1093–F1099.

Pajor, A.M., and N.N. Sun. 2000. Molecular cloning, chromosomal organization, and functional characterization of a sodium-dicarboxylate cotransporter from mouse kidney. *Am. J. Physiol. Renal Physiol.* 279:F482–F490.

Pajor, A.M., and N.N. Sun. 2013. Nonsteroidal anti-inflammatory drugs and other anthranilic acids inhibit the Na^+/dicarboxylate symporter from *Staphylococcus aureus*. *Biochemistry.* 52:2924–2932. http://dx.doi.org/10.1021/bi301611u

Pajor, A.M., N.N. Sun, and A. Leung. 2013. Functional characterization of SdcF from *Bacillus licheniformis*, a homolog of the SLC13 Na^+/dicarboxylate transporters. *J. Membr. Biol.* 246:705–715. http://dx.doi.org/10.1007/s00232-013-9590-3

Quick, M., H. Yano, N.R. Goldberg, L. Duan, T. Beuming, L. Shi, H. Weinstein, and J.A. Javitch. 2006. State-dependent conformations of the translocation pathway in the tyrosine transporter Tyt1, a novel neurotransmitter:sodium symporter from *Fusobacterium nucleatum*. *J. Biol. Chem.* 281:26444–26454. http://dx.doi.org/10.1074/jbc.M602438200

Reyes, N., C. Ginter, and O. Boudker. 2009. Transport mechanism of a bacterial homologue of glutamate transporters. *Nature.* 462:880–885. http://dx.doi.org/10.1038/nature08616

Rogina, B., R.A. Reenan, S.P. Nilsen, and S.L. Helfand. 2000. Extended life-span conferred by cotransporter gene mutations in *Drosophila*. *Science.* 290:2137–2140. http://dx.doi.org/10.1126/science.290.5499.2137

Ruderman, N.B., A.K. Saha, D. Vavvas, and L.A. Witters. 1999. Malonyl-CoA, fuel sensing, and insulin resistance. *Am. J. Physiol.* 276:E1–E18.

Ryan, R.M., and J.A. Mindell. 2007. The uncoupled chloride conductance of a bacterial glutamate transporter homolog. *Nat. Struct. Mol. Biol.* 14:365–371. http://dx.doi.org/10.1038/nsmb1230

Ryan, R.M., E.L. Compton, and J.A. Mindell. 2009. Functional characterization of a Na^+-dependent aspartate transporter from *Pyrococcus horikoshii*. *J. Biol. Chem.* 284:17540–17548. http://dx.doi.org/10.1074/jbc.M109.005926

Saier, M.H., Jr., C.V. Tran, and R.D. Barabote. 2006. TCDB: the Transporter Classification Database for membrane transport protein analyses and information. *Nucleic Acids Res.* 34:D181–D186. http://dx.doi.org/10.1093/nar/gkj001

Spencer, A.F., and J.M. Lowenstein. 1962. The supply of precursors for the synthesis of fatty acids. *J. Biol. Chem.* 237:3640–3648.

Stein, W.D. 1986. Transport and Diffusion across Cell Membranes. Academic Press, New York. 704 pp.

Strickler, M.A., J.A. Hall, O. Gaiko, and A.M. Pajor. 2009. Functional characterization of a Na^+-coupled dicarboxylate transporter from *Bacillus licheniformis*. *Biochim. Biophys. Acta.* 1788:2489–2496. http://dx.doi.org/10.1016/j.bbamem.2009.10.008

Verdon, G., and O. Boudker. 2012. Crystal structure of an asymmetric trimer of a bacterial glutamate transporter homolog. *Nat. Struct. Mol. Biol.* 19:355–357. http://dx.doi.org/10.1038/nsmb.2233

Wang, H., Y.J. Fei, R. Kekuda, T.L. Yang-Feng, L.D. Devoe, F.H. Leibach, P.D. Prasad, and V. Ganapathy. 2000. Structure, function, and genomic organization of human Na^+-dependent high-affinity dicarboxylate transporter. *Am. J. Physiol. Cell Physiol.* 278:C1019–C1030.

Wright, S.H., I. Kippen, and E.M. Wright. 1982. Stoichiometry of Na^+-succinate cotransport in renal brush-border membranes. *J. Biol. Chem.* 257:1773–1778.

Yernool, D., O. Boudker, Y. Jin, and E. Gouaux. 2004. Structure of a glutamate transporter homologue from *Pyrococcus horikoshii*. *Nature.* 431:811–818. http://dx.doi.org/10.1038/nature03018

Youn, J.W., E. Jolkver, R. Krämer, K. Marin, and V.F. Wendisch. 2008. Identification and characterization of the dicarboxylate uptake system DccT in *Corynebacterium glutamicum*. *J. Bacteriol.* 190:6458–6466. http://dx.doi.org/10.1128/JB.00780-08